Cell Reports
Physical Science

CellPress

Article

Dispersion and Stabilization of Alkylated 2D MXene in Nonpolar Solvents and Their Pseudocapacitive Behavior

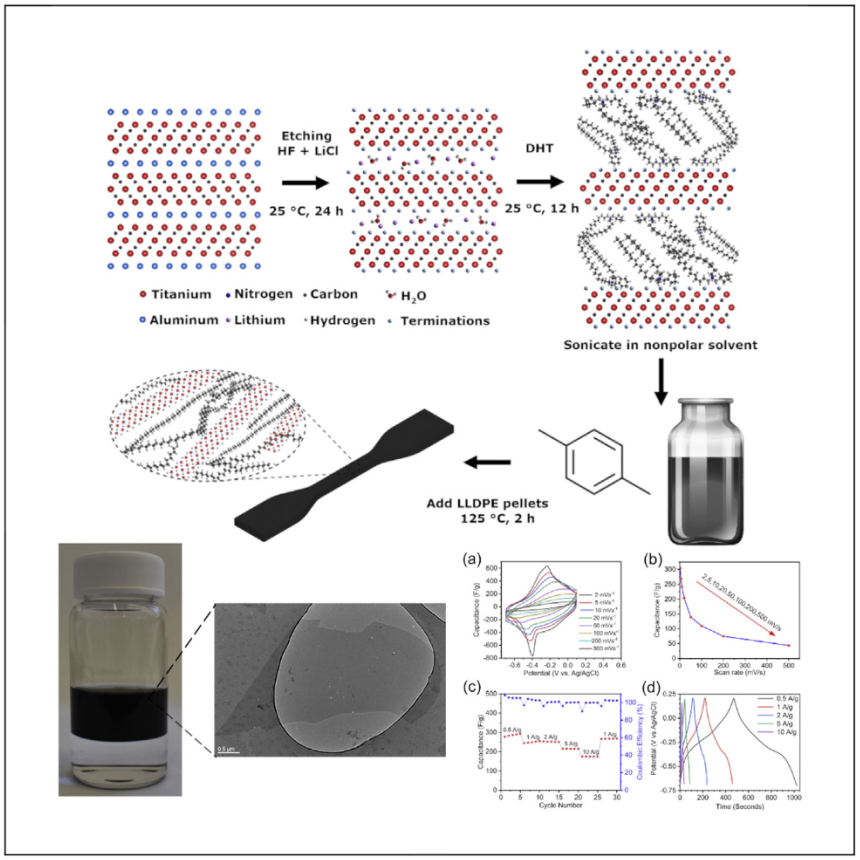

Carey et al. report the surface-modified organophilic $Ti_3C_2T_z$ MXene, which forms stable suspensions in nonpolar solvents. This method is used to prepare polyethylene nanocomposites, where the ready dispersion of DHT-MXene results in enhanced mechanical properties. In addition, films made from these DHT-MXene suspensions can be used as electrodes that exhibit pseudocapacitive behavior.

Michael Carey, Zachary Hinton, Varun Natu, ..., Nicolas J. Alvarez, Vibha Kalra, Michel W. Barsoum

barsoumw@drexel.edu

HIGHLIGHTS

MXene multilayers are exfoliated and dispersed in nonpolar solvents

These two-dimensional nonpolar dispersions have high colloidal and oxidation stability

This method is used to prepare nanocomposites with improved mechanical properties

The electrochemical properties of these modified MXene films are evaluated

Carey et al., Cell Reports Physical Science *1*, 100042
April 22, 2020 © 2020 The Author(s).
https://doi.org/10.1016/j.xcrp.2020.100042

Cell Reports
Physical Science

CellPress

Article

Dispersion and Stabilization of Alkylated 2D MXene in Nonpolar Solvents and Their Pseudocapacitive Behavior

Michael Carey,[1] Zachary Hinton,[2] Varun Natu,[1] Rahul Pai,[2] Maxim Sokol,[1] Nicolas J. Alvarez,[2] Vibha Kalra,[2] and Michel W. Barsoum[1,3,4,*]

SUMMARY

To date, MXene dispersions have been mostly limited to polar solvents. Here, we show that when the lithium cations present between MXene multilayers after etching are exchanged with di(hydrogenated tallow)benzyl methyl ammonium chloride (DHT), they become organophilic and form highly stable colloidal suspensions in nonpolar solvents. The rapid cation exchange occurs under ambient conditions and the resulting two-dimensional flakes are well dispersed and remain oxide free. A 142 $\pm$ 0.7-μm thick film ($\approx$10 mg $\cdot$ cm^{-2}) made from a DHT-$Ti_3C_2T_z$ suspension in toluene exhibits pseudocapacitive behavior, with a capacitance of 305 F $\cdot$ g^{-1} at a scan rate 2 mV $\cdot$ s^{-1}. The moduli and tensile strengths of solution-processed polyethylene nanocomposites are increased by $\approx$11% and 32% with a loading of $\approx$1 vol% DHT-$Ti_3C_2T_z$. Our approach may enable the use of MXenes in multiple research and industrial fields.

INTRODUCTION

Among two-dimensional (2D) materials, MXenes have garnered significant interest lately due to their unique combination of properties, particularly hydrophilicity and conductivity. The name MXene arises as they are derived from the MAX phases, and their 2D nature and conductivity liken them to graphene. Unlike graphene, MXenes offer a greater range of chemical compositions, and to date, >30 different MXenes have been synthesized.[1] MXenes have found use in research fields, including electronics, composites, energy storage, and catalysis.[1] However, many practical challenges associated with their synthesis, handling, and storage remain. For example, their hydrophilicity limits their use in a broader chemical sense, as only polar solvents such as water, ethanol, dimethylsulfoxide (DMSO), dimethylformamide (DMF), and others are suitable. In addition, MXenes are susceptible to oxidation, limiting their ability to be stored for any meaningful amounts of time, especially in aqueous suspensions. However, this is an ongoing field of research, and recent breakthroughs have allowed for longer-term stabilities in aqueous media.[2,3]

MXenes, for the most part, come in two physical forms, multilayer powders or colloidal suspensions comprising single flakes to a few flakes. The latter are typically obtained by sonicating multilayers in a solution and subsequently separating the colloidal supernatant from the multilayer sediment by centrifugation. This results in a dark suspension, with MXene concentrations typically as high as 20 g L^{-1}.[1] To date most, if not all, of this work has been carried out in polar solvents, including water.

[1]Department of Materials Science and Engineering, Drexel University, 3141 Chestnut St., Philadelphia, PA 19104, USA

[2]Department of Chemical and Biological Engineering, Drexel University, 3141 Chestnut St., Philadelphia, PA 19104, USA

[3]Twitter: @DrexelMaterials

[4]Lead Contact

*Correspondence: barsoumw@drexel.edu

https://doi.org/10.1016/j.xcrp.2020.100042

However, many chemical processes such as liquid-liquid extractions, polymerization reactions, and reagent or product purification, and storage and handling require the use of nonpolar solvents. For example, the stability of graphene and graphene oxide in nonpolar solvents has been extensively studied, namely by the reduction of graphene oxide,[4] selective use of solvent,[5] or alkyl functionalization,[6–8] or through a combination of these techniques. Given the unique properties of MXenes, which combine those of layered clays and graphene, namely ion intercalation, electronic conductivity, and hydrophilicity, they may also find use in these fields if they can be dispersed in nonpolar solvents. To date, little work has been done on dispersing MXene in nonpolar solvents. Lim et al. were able to form suspensions of silanized $Ti_3C_2T_z$ in n-hexane.[9] However, this method required the use of very-high-molecular-weight emulsifying agents such as poly(2-acrylamido-2-methyl-1-propanesulfonic acid) (MW 800,000 g • mol^{-1}), in addition to the surface agent octyltriethoxysilane, so the final alkylsilane mass content was 45.1 wt%. This process also used already sonicated and delaminated $Ti_3C_2T_z$ colloidal suspensions, elevated temperatures, use of ammonia, and several sonication steps.[9]

Over the past 5 years, we have repeatedly shown that MXenes and clays share many commonalities.[10–14] Like clays, MXenes form stable aqueous colloidal suspensions around neutral pH[15] and contain exchangeable cation, which can expand the interlayer space upon their introduction.[13] The interlayer space can also contain water, and the spacing of these layers is a function of humidity.[13,15–17] This article continues in that vein, using $Ti_3C_2T_z$ multilayers that can be produced on a much larger scale than delaminated, colloidal suspensions.

Layered silicates such as montmorillonite, kaolinite, or mica do not readily disperse in nonpolar solvents. However, when the clay layers are intercalated with n-alkyl ammonium cations, they disperse readily and remain stably suspended. Such suspensions have been found to be rather useful in many practical applications such as oil-based drilling fluids, lubricating greases, inks, and paints in which the clay acts as a rheological control agent.[18] Unlike clays, however, the charges in MXene are due to the average oxidation states of the transition metal and X element, whereas charges in clays are due to the substitution of Si by aliovalent cations, typically Al.[19] In regard to the use of MXenes in polymer-based composites, we have shown that the cations present between MXene sheets can be exchanged with organic ions such as 12-aminolauric acid (ALA) or di(hydrogenated tallow)benzyl methyl ammonium chloride (DHT) to disperse $Ti_3C_2T_z$ multilayers in nylon-6[20] and epoxy matrices.[21]

The purpose of this work was to delineate a simple, scalable, and inexpensive strategy to disperse and stabilize $Ti_3C_2T_z$ flakes in nonpolar solvents. The key is to replace the cations present between the multilayers after the etching and washing steps with DHT, a common, inexpensive, and industrially relevant quaternary alkyl ammonium surfactant.

RESULTS AND DISCUSSION

Synthesis and Characterization of DHT-Modified $Ti_3C_2T_z$

The details of synthesizing DHT-modified $Ti_3C_2T_z$ and their subsequent dispersion in deionized (DI) water, ethanol, DMSO, decahydronaphthalene (decalin), chloroform, hexane, cyclohexane, toluene, and p-xylene can be found in the Experimental Procedures section and are illustrated in Scheme 1. In short, Li^+ ions present in the multilayer intergallery space after etching and washing are ion exchanged with DHT. The

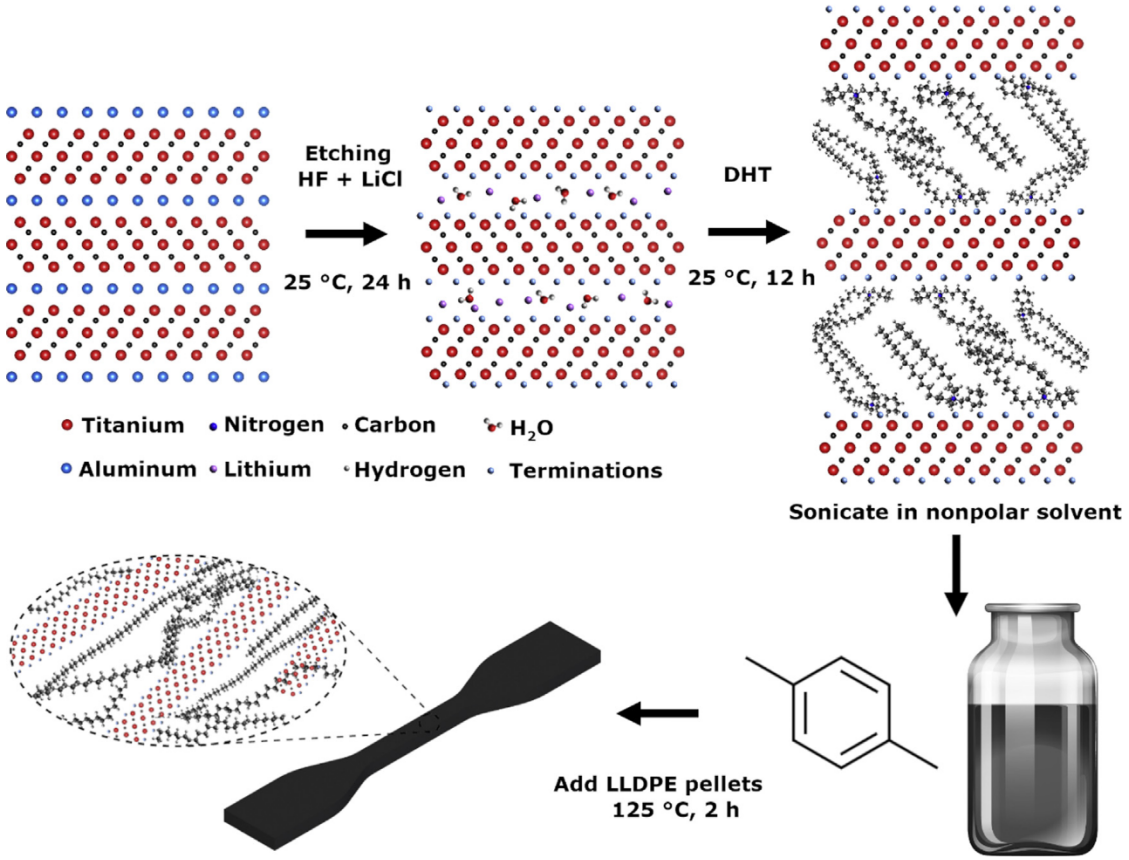

Scheme 1. Processing Steps

Schematic illustration of Ti_3AlC_2 etching, treatment of obtained $Ti_3C_2T_z$ multilayers with DHT, dispersion in a nonpolar solvent, and their use in solution processing of linear low-density polyethylene nanocomposite specimens.

resulting multilayers are then readily dispersible in nonpolar solvents (Figure 1A). Once dispersed, the suspensions were monitored over the course of 10 days. The DHT-treated multilayers not only dispersed readily in the aforementioned nonpolar solvents but also these suspensions were stable for at least 10 days (Figure 1B. It is not surprising, then, that the non-treated multilayers were only dispersible in polar solvents (Figures 1C and 1D).

After several hours, the suspension containing the untreated MXene in DI water and DMSO became more transparent, indicating that some settling had begun, which continued until the suspension was completely transparent <12 h later. In that respect, the fact that DHT-MXene suspensions are stable in nonpolar solvents, even after 10 days, is noteworthy. In one case, multilayers were dispersed in a water-decalin solution and shaken before allowing the system to rest. After a few minutes, the MXene was found exclusively in the decalin that formed a liquid-liquid aqueous and organic interface between water and decalin (see inset of Figure 5). This configuration remained stable for >30 days. It follows that the dispersion-exfoliation of DHT-treated $Ti_3C_2T_z$ multilayers in nonpolar solvents is highly stable. This stability is attributed to the organophilic nature of DHT-$Ti_3C_2T_z$, as the long alkyl chains of DHT enhance the chemical compatibility in these solvents. Dynamic light scattering results indicate that the average MXene particle size is between 150 and 400 nm (Figure S1) and is dependent upon the solvent used.

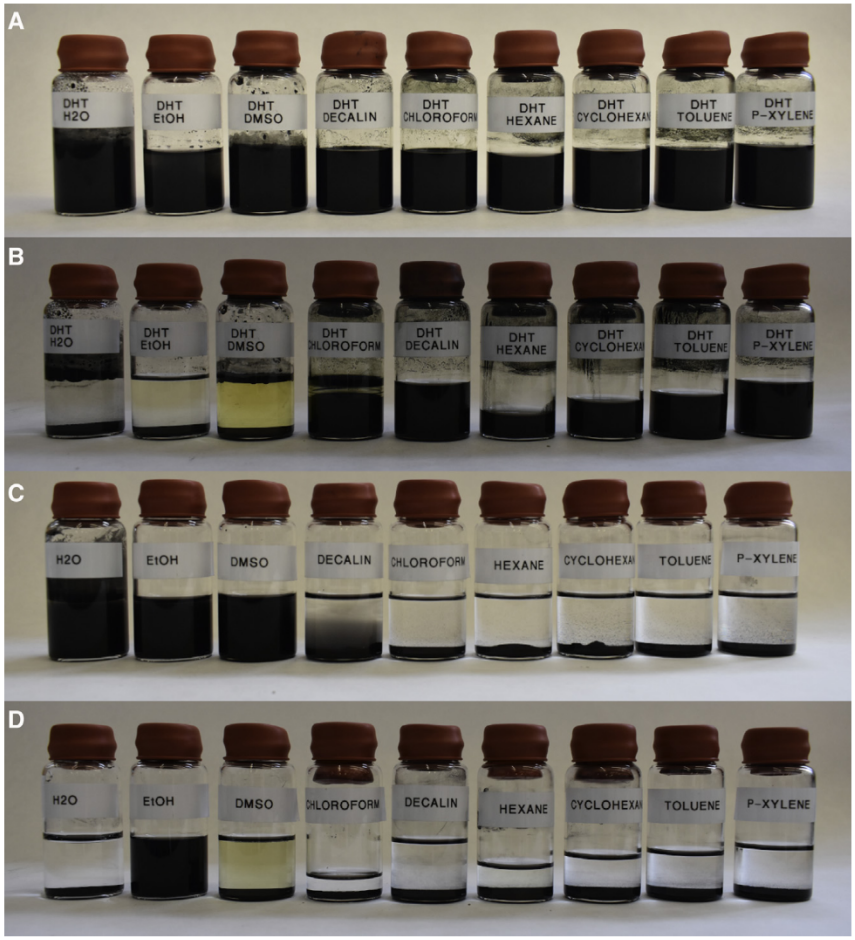

Figure 1. Photographs of $Ti_3C_2T_z$ Suspensions in Polar (First Three Vials) and Nonpolar Solvents
(A) DHT treated just after sonication.
(B) Same as (A), but after 10 days.
(C) Untreated just after sonication.
(D) Untreated after 10 days.
The reduced liquid level in some of the containers is due to solvent evaporation.

After this time, suspensions were isolated via centrifugation at 3,500 rpm (2,301 relative centrifugal force [RCF]) for 1 min and vacuum filtered to obtain filtered films (FFs). X-ray diffraction (XRD) patterns of these films (Figure 2A) are compared to pristine, as-synthesized MXene, DHT-MX, and FFs after dispersing in chloroform, decalin, hexane, cyclohexane, toluene, and p-xylene. We also obtained the XRD patterns of the sediments after centrifugation (Figure S2) and after drying the FF in vacuum at 200°C for 24 h (Figure S3). All basal spacings, d_{002}, are plotted in Figure 2B. From these results, the following is salient:

(1) After the hydrofluoric acid (HF)-lithium chloride (LiCl) etching step, d_{002} is 14.6 Å (Figure 2A). Replacing the Li^+ with DHT increases d to 36.7 Å (Figure 2B), which agrees with the basal spacings of n-alkylammonium-treated nanoclays.[22]
(2) The d-spacings of the sediments depend on solvent (red columns in Figure 2B). For chloroform and hexane, d_{002} drops compared to the DHT-treated powders, for cyclohexane d_{002} remains the same, and for decalin, toluene, and p-xylene the d-spacings expand to >50 Å.

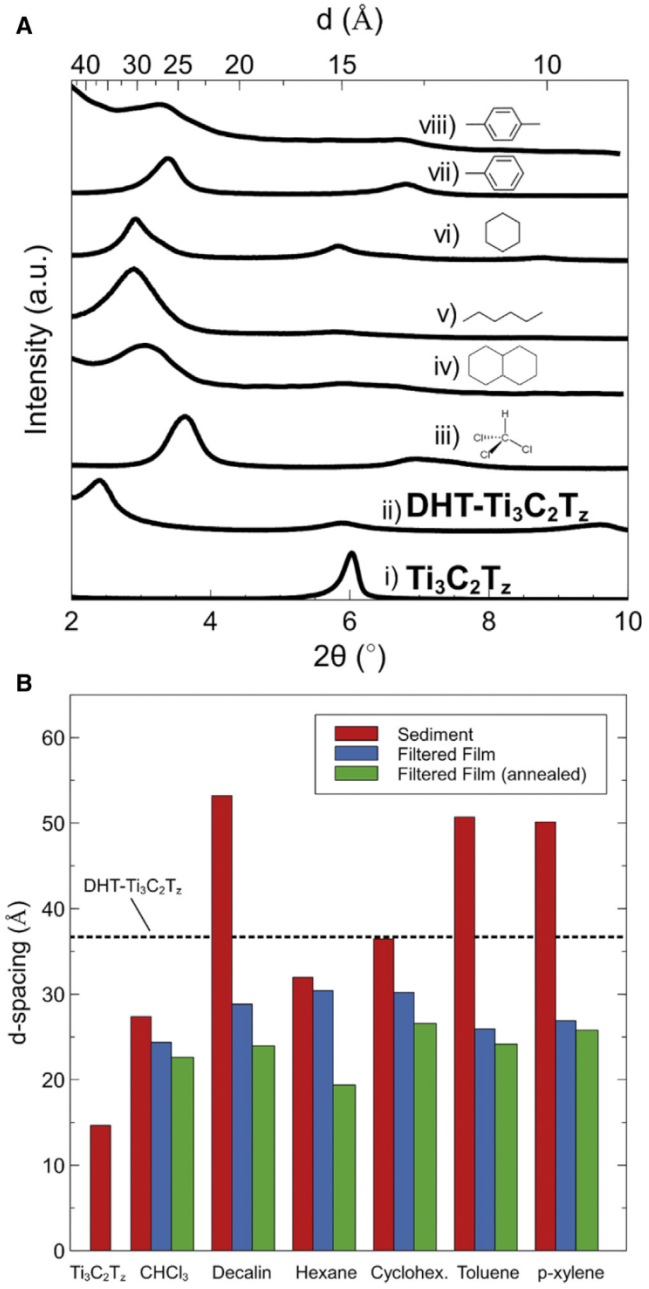

Figure 2. XRD Measurements

(A) Low-angle XRD patterns of (i) multilayers after etching and washing, (ii) DHT-treated multilayers, and filtered films of suspensions in, (iii) chloroform, (iv) decalin, (v) hexane, (vi) cyclohexane, (vii) toluene, and (viii) p-xylene. Top x axis shows the spacing between layers in angstroms. Structures of the solvent molecules are shown as insets.

(B) d-Spacing as a function of solvent for sediment (red), filtered films (blue), and filtered films after drying at 200°C for 24 h (green). The horizontal line is d-spacing after treatment with DHT. d-spacing after etching is 14.6 Å (leftmost bar).

(3) The d-spacings of the FF (blue columns in Figure 2B) are less than those of the sediments. In some cases, the drops are quite large. For example, for decalin, d_{002} drops from >50 Å to <30 Å. This drop is due to the evaporation of the solvent.

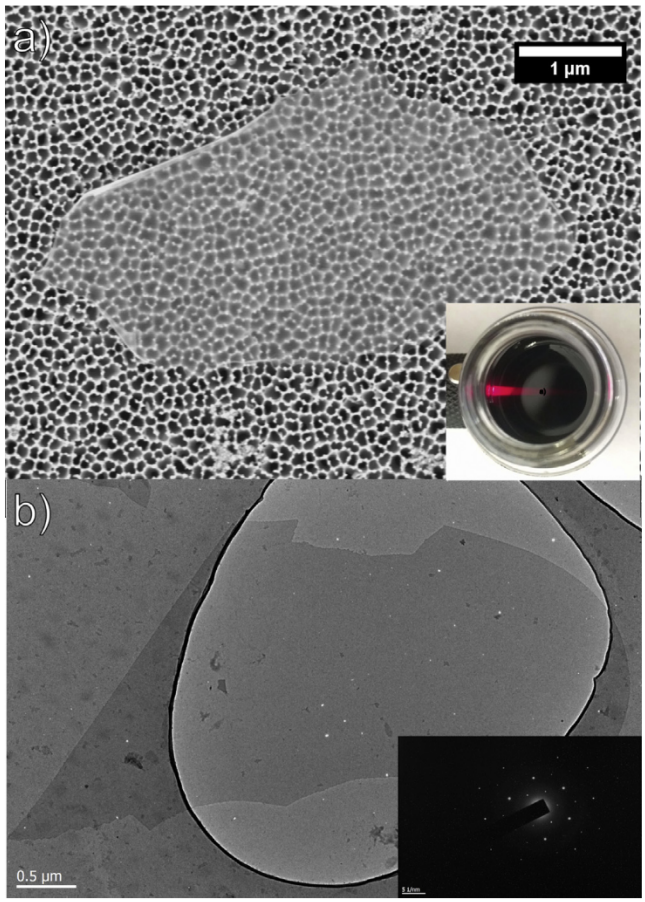

Figure 3. Electron Microscopy

(A) Typical SEM micrograph of a drop of DHT-treated $Ti_3C_2T_z$ dispersed in a cyclohexane suspension cast on a porous alumina substrate. Scale bar, 1 µm. Inset shows the Tyndall effect.
(B) TEM micrograph of a drop of a DHT-MXene-decalin suspension after 10 days. Scale bar, 0.5 µm. Inset shows selected area diffraction pattern with a scale bar of 10 nm^{-1}.

(4) It is not surprising that drying the FF at 200°C for 24 h reduces the d-spacings (green columns in Figure 2B) to their minimal values, which hover between 19 and 27 Å. This decrease is attributable to further evaporation of the solvents.

Scanning electron microscopy (SEM) micrographs of a DHT-MX-cyclohexane suspension drop-cast on porous alumina substrates confirm that at least some of these flakes comprise few layers (Figure 3A). This colloidal nature is evidenced by the Tyndall effect observed in the DHT-MXene-cyclohexane suspension (Figure 3A, inset). SEM micrographs for other solvents can be found in Figure S4.

A typical transmission electron microscopy (TEM) micrograph of an aliquot of the DHT-MXene-cyclohexane suspension, drop-cast on a TEM grid (Figure 3B), confirms that the suspension contains few-flake MXenes that retain the hexagonal crystal structure of their parent MAX phase, Ti_3AlC_2, as evidenced by the selected area diffraction of the MXene flake (Figure 3B, inset). Just as important, the flakes show no signs of oxidation, despite being in suspension for >10 days. TEM micrographs for other solvents can be found in Figure S5. In contradistinction, storing $Ti_3C_2T_z$ flakes in water for even <10 d results in significant oxidation.[2]

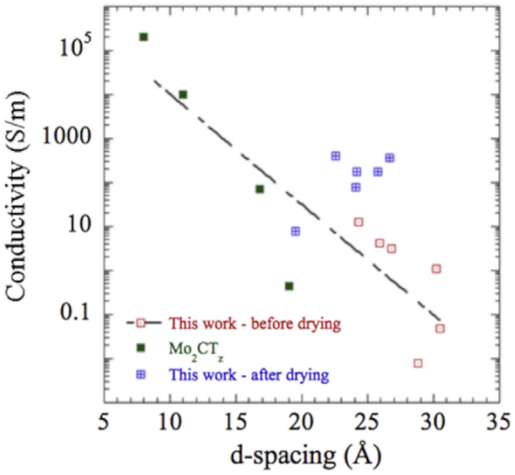

Figure 4. Effect of Solvent and d-Spacing on Conductivity

Effect of solvent and d-spacing on conductivity of filtered films (before drying [red] and after drying [blue]). Also plotted are the results for Mo_2CT_z films.[23]

The room temperature four-point DC conductivities, σ, of the FF before and after drying in vacuum at 200°C for 24 h, are plotted in Figure 4. From this plot, one can conclude that the conductivity (1) is a strong function of d-spacing before annealing, but less so after annealing; (2) is a function of what is between the layers; and (3) is greatly enhanced by mild heating in a mechanical vacuum at 200°C for 24 h (blue squares in Figure 4). Also plotted in Figure 4 are previous results (green squares) on Mo_2CT_z-filtered films.[23] A least-squares fit of all of these results (excluding the annealed films, viz. blue excluding) yields the following relation:

$$\log_{10}\sigma(S/m) = 6.5 - 0.25 \cdot d_{002}\left(\text{Å}\right), R^2 = 0.78 \qquad \text{(Equation 1)}$$

Fitting the log plot yields:

$$\sigma(S/m) = 3.2 \times 10^6 \cdot exp^{-0.6 \cdot d_{002}} \qquad \text{(Equation 2)}$$

This exponential dependence on d_{002} has been observed before in Mo_2CT_z FFs and clearly implicates interflake transport as being rate limiting.

Upon drying, the response (blue squares in Figure 4) becomes a much weaker function of d-spacing, suggesting that percolation paths develop between the flakes. This is not surprising since it is reasonable to assume that upon drying, the d-spacings are no longer uniform. Values of the d spacings and conductivities before and after annealing, can be found in Table S1.

The MXene concentrations in our suspensions were measured by heating the FFs to 200°C for 24 h in vacuum and weighing the resulting films. A plot of concentration as a function of the Hildebrand solubility parameter (δ) of the respective solvents is shown in Figure 5. The Hildebrand solubility parameter, δ, is defined as the square root of the cohesive energy density and can also be described by the square root of the sum of squares of the dispersive, hydrogen bonding, and polar Hansen solubility parameters given by δ_D, δ_H, and δ_P, respectively, as

$$\delta = \sqrt{\frac{\Delta H_v - RT}{V_m}} = \sqrt{\delta_D^2 + \delta_H^2 + \delta_P^2} \qquad \text{(Equation 3)}$$

where ΔH_v, R, T, and V_m are the heat of vaporization, gas law constant, temperature, and molar volume of the condensed phase, respectively. A near-Gaussian trend (Figure 5) can be established, with p-xylene yielding the highest concentration,

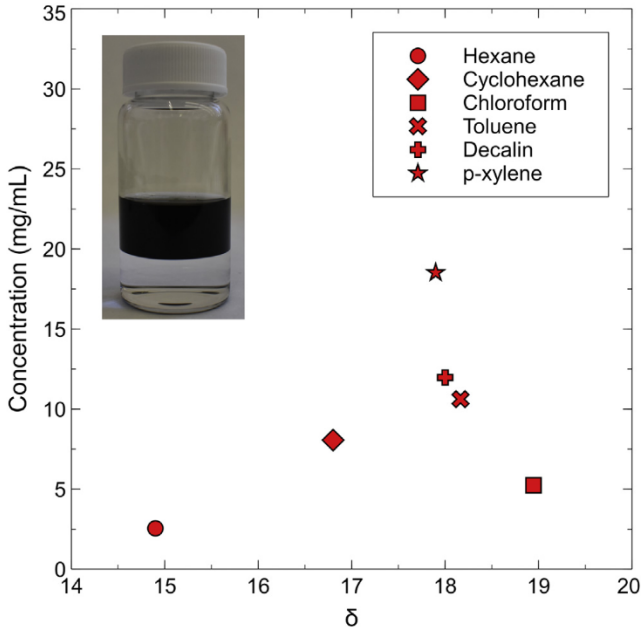

Figure 5. Concentration as a Function of the Hildebrand Solubility

Concentration of DHT-$Ti_3C_2T_z$ in nonpolar suspensions as a function of the Hildebrand solubility parameter (δ), obtained or calculated from references values.[26] Inset is a photo of 10 mL DHT-$Ti_3C_2T_z$ in decalin on top of 10 mL deionized water, demonstrating the liquid-liquid interface. This sample remained unchanged after 30 days.

suggesting that DHT-$Ti_3C_2T_z$ is most stable in solvents with a δ of ~18 $MPa^{1/2}$, as opposed to the ~27 $MPa^{1/2}$ that is optimal for untreated $Ti_3C_2T_z$ in polar solvents.[24] Carbon nanotubes are most stable in solvents with δ ~23 $MPa^{1/2}$, which reduces to ~19.5 $MPa^{1/2}$ upon functionalization of these nanotubes with octadecylamine.[25]

Comparison of attenuated total reflection-Fourier transform infrared spectroscopy (ATR-FTIR) spectra of solvents and DHT-MX suspensions indicates that all of the functional groups and vibrations of the respective solvent remain. However, slight redshifts in the DHT-MX suspensions suggest interactions between DHT-MXenes and solvent (Figure S6).

Potential Applications

To demonstrate a potential application of our method, solution-processed, linear, low-density polyethylene (LLDPE) nanocomposites were made, starting with DHT-MXene multilayers. It was found that mechanical reinforcement of the host LLDPE loaded with only 1.12 vol% DHT-functionalized $Ti_3C_2T_z$ resulted in an 11% increase in elastic moduli and a 32% increase in the maximum tensile strength. For untreated MXene composites, a 2% decrease in moduli and a 9.2% increase in maximum tensile strength were observed. Representative stress-strain behavior can be seen in Figure 6, and all of the samples can be seen in Figure S7.

Thermogravimetric analysis (TGA) revealed that the DHT content in the DHT-$Ti_3C_2T_z$ powders was ~26.5 wt% (Figure S8), after adjusting for the small amount of residual water content lost at temperatures <200°C. In addition, both treated and untreated MXene-containing samples were found to have the same targeted MXene load, 5 wt % (Figure S8). This weight fraction is equivalent to 1.12 vol %. Furthermore, the degradation temperature, T_D (taken as the temperature at which the derivative of

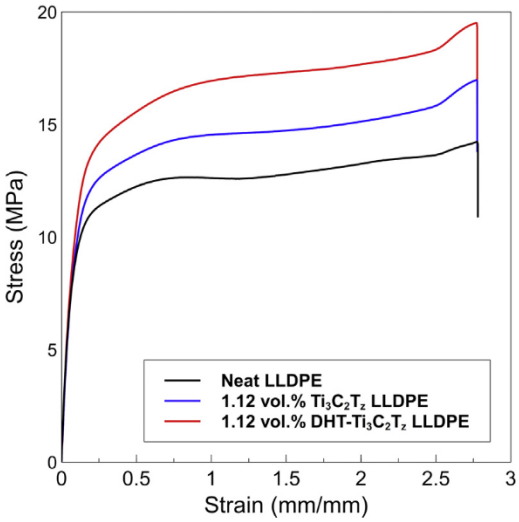

Figure 6. Stress-Strain Curves
Maximum stress-strain curves of neat LLDPE (black) and composite samples with 1.12 vol% DHT-$Ti_3C_2T_z$ (red) and untreated $Ti_3C_2T_z$ (blue).

weight loss with respect to temperature is maximized) was increased from 464.5°C in the neat LLDPE to 477.2°C and 478.4°C in untreated and treated specimens, respectively (see Figure S9). Digital photographs of composite pellets can be found in Figure S10.

Melt rheology was used to further probe the effects of the DHT treatment on the MXene-LLDPE nanocomposites. The master curves of storage (G′) and loss (G″) moduli as well as complex (measured in oscillatory shear) viscosity are shown in Figures 7A and 7B as a function of angular frequency at a reference temperature of 200°C. For the untreated MXene, the response is nearly identical to the neat LLDPE. This is expected as the low-volume fraction of particles makes very little contribution to stress in the aggregated (low aspect ratio) state. However, the DHT-treated MXene-LLDPE melt shows noticeably higher values of G′, G″, and complex viscosities at the lower frequencies. This indicates a slowed chain reptation for DHT-MXene-LLDPE melts. This likely arises from one or more of the following mechanisms: decrease in the characteristic length scale of particles that hinder reptation or increase in particle-polymer contacts or DHT-polymer interaction at or near the MXene surfaces.[27] This occurs without the typical indication of percolation (0.1 vol %),[28] which may indicate that DHT inhibits percolation, possibly due to repulsive forces between the alkyl chains, as seen with other grafted nanoparticles.[27] The dispersion of DHT-MXene in LLDPE is supported by the lack of a Ti K_α energy-dispersive X-ray spectroscopy (EDS) signal of DHT-$Ti_3C_2T_z$-containing LLDPE specimens (Figure S11). Note that such a signal is present when the multilayers are not DHT-treated (compare Figures S11b and S11c). At higher frequencies, there is no difference between the three melts.

One of the more promising applications for MXenes is as electrodes in supercapacitors.[29] To further demonstrate the usefulness of our approach, we filtered toluene-dispersed DHT-MXenes to make freestanding films with a high mass loading of ≈10 mg • cm^{-2} and a thickness of ≈140 μm. This thickness was chosen as it is within the normal range of electrode thickness in the supercapacitor field. This particular system was chosen because the produced freestanding films were mechanically robust and exhibited reasonable conductivity. The experimental details are outlined in the Experimental Procedures. Briefly, we used a 3-electrode setup in 3 M H_2SO_4 electrolyte with DHT-$Ti_3C_2T_z$ as the working electrode,

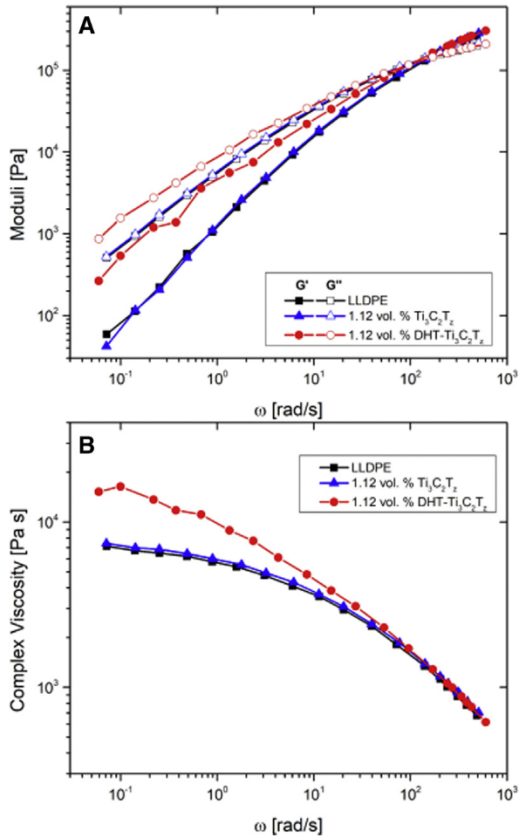

Figure 7. Melt Rheology

(A and B) Effect of frequency on (A) G′ and G″ and (B) complex viscosity of the three melts represented as master curves at T_{ref} = 200°C.

overcapacitive activated carbon as the counter electrode, and Ag/AgCl in 1 M KCl solution as the reference electrode. The practical industrial level mass loadings and packing densities achieved in such filtered films cause re-stacking of the layers, which can limit accessible sites, and hence, measured capacitances. To enable enhanced electrolyte access to the MXene flakes and mitigate the aforementioned challenge, the FF electrodes were pre-cycled for 5,000 cycles at 20 mV • s^{-1} (see Figure S12A) before testing their electrochemical behavior. As expected, the capacitance increased with cycling, first rapidly and then later at a steadier rate of increase, finally stabilizing at a near-constant value. Specifically, the capacitance increases from 50 F • g^{-1} in cycle 1 to >200 F • g^{-1} after 5,000 cycles (see Figure S12B).

When the electrodes were cycled at various scan rates (Figure 8A) the cathodic and anodic peak separation was ~170 mV at 2 mV • s^{-1}, which increased to ~300 mV at 20 mV • s^{-1}. Figure 8B plots the capacitance as a function of scan rate. The electrode displays capacitances of 305, 272, 240, 205, 140, 118, 75, and 50 F • g^{-1} at 2, 5, 10, 20, 50, 100, 200, and 500 mV • s^{-1}, respectively. The sharp drop, as a function of scan rate, is expected due to the higher packing volume density of our electrodes. Figure 8C shows the rate performance at various current densities. The electrode demonstrates a capacitance of ~280, 266, 253, 225, and 185 F • g^{-1} at 0.5, 1, 2, 5, and 10 A • g^{-1}, respectively. The electrode regains 95% of its capacitance when cycled again at 1 A • g^{-1}. Figure 8D shows the galvanostatic charge

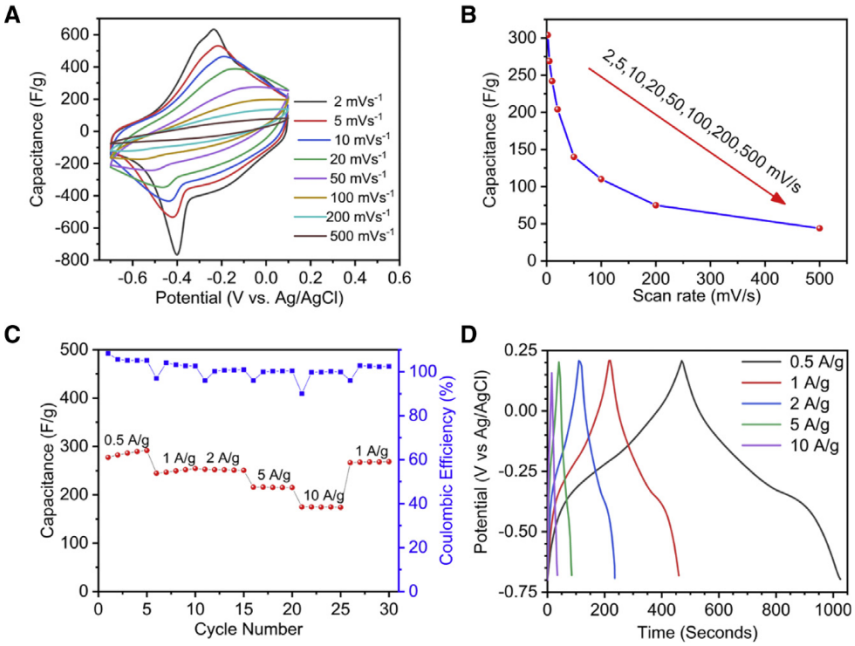

Figure 8. Electrochemical Characteristics

Electrochemical characteristics of DHT-MXene pre-dispersed in toluene electrode and 3 M H_2SO_4 electrolyte.

(A) Cyclic voltammetry curves as a function of scan rates.

(B) Capacitance as a function of scan rates.

(C) Rate performance at various current densities.

(D) Cyclic charge-discharge curves at various current densities.

All of the measurements were conducted with freestanding DHT-MXene electrodes with ≈10 mg • cm^{-2} loading and a thickness of 142 ± 0.7 μm.

discharge curves at various current densities. The behavior of these curves is in agreement with the cyclic voltammetry (CV) results and further corroborate the presence of pseudocapacitive behavior. The maximum capacitance of 280 F • g^{-1} was observed at 0.5 A • g^{-1} which decreased to 185 F • g^{-1} at 10 A • g^{-1} due to the expected diffusion limitation, and hence underutilization, of the active material with increasing rate. It is worth noting that 96% of the capacitance of the first cycle at 1 A • g^{-1} was regained after the high current excursions (Figure 8C). Furthermore, DHT-MXene retained 97% of the initial specific capacitance when cycled at 1 A • g^{-1} over 100 cycles (post- and pre-cycling).

To place our numbers in perspective, we compared them with relevant previous works on Ti_3C_2 (Table 1). Our numbers stand out in two respects. First, in the loading; our samples are the highest by a factor of at least two compared to previous works. Second, despite high mass loading and packing density, which are critical parameters for practical device-level performances, our capacitance numbers are reasonable and comparable to many other water-processed films. Lastly, it is crucial to note that the motivation for such electrochemical measurements is not to understand how or what factors affect the supercapacitance of our devices, but rather to unambiguously show that despite the DHT treatment and the concomitant increase in resistance of our FF, their response to cycling in H_2SO_4 is comparable to conventional electrodes made with water. If optimized appropriately, many of our materials can be used successfully in electrochemical applications.

Table 1. Electrochemical Parameters and Gravimetric Capacitances for This and Previous Work at Scan Rate of 2 mV · s^{-1}

Material(s)	Electrolyte	Potential Window, ΔV, in V	Capacitance, C (F · g^{-1})	Energy Density CΔV^2 (J · g^{-1})	Loading	Reference
$Ti_3C_2T_z$	1 M H_2SO_4	0.4	99	79.8	3 mg · cm^{-2}	33
$Ti_3C_2T_z$	1 M H_2SO_4	0.6	325	117	2.6 mg	34
$Ti_3C_2T_z$ clay	1 M H_2SO_4	0.55	245	74.1	3.6–3.8 mg · cm^{-3}	10
$Ti_3C_2T_z$	3 M H_2SO_4	1	330	330	3.7 mg · cm^{-3}	35
DHT-Ti_3C_2	3 M H_2SO_4	0.8	305	195	≈10 mg · cm^{-2}	Present article

Lastly, we plot the X-ray photoelectron spectroscopy (XPS) spectra of the Ti, F, C, and O regions, obtained on powders, before and after DHT treatment, in Figures S13 and S14, respectively. The results are summarized in Table S2. No significant change was observed in the Ti region before and after DHT treatment. After DHT treatment, the C-C/C-H content goes up slightly, which is probably indicative of the presence of DHT in MXene, due to its high C content. The TiO_2 content was observed to increase after DHT treatment, possibly due to the prolonged exposure to water during DHT intercalation. Finally, the biggest difference is seen in the photoelectron spectra of F, where a new peak is seen after DHT treatment at ~683.4 eV. This is possibly due to the reaction of DHT with the F terminations, but this change is not reflected in the Ti region, so the reason behind the emergence of the new peak is still unclear. More work needs to be done to understand the interaction of DHT with the F terminations, which is beyond the scope of the present work. The chemistry and surface terminations, typically denoted as T_z, were determined to be $Ti_3C_{1.8}O_{1.8}OH_{1.1}F_{0.4}$ before and $Ti_3C_{3.5}O_2OH_{0.61}F_{2.4}$ after DHT treatment. Why the sum of the terminations moles is >2 is not clear at this time.

We believe this work advances the field of MXene research, particularly when the history of this field is considered. The first generation of $Ti_3C_2T_z$ that was HF etched was only dispersible after intercalating the multilayers with DMSO or tetrabutylammonium hydroxide (TBAOH).[30,31] The second breakthrough occurred when we showed that if the etching solution is LiF/HCl instead of HF, then it was possible to disperse MXenes in water without any other additives.[10] Given the stability in water, it was not long before it was discovered that $Ti_3C_2T_z$ was dispersible and stable in other polar solvents.[24] What has to date been lacking, however, was a facile, scalable, rapid, and inexpensive method to disperse $Ti_3C_2T_z$ in nonpolar solvents. With this work, we show that is possible, which will undoubtedly further enhance the application space of MXenes, especially in ones where hydrophobicity is required.

In summary, multilayers of $Ti_3C_2T_z$ were dispersed and stabilized in nonpolar solvents, namely chloroform, decalin, hexane, cyclohexane, toluene, and p-xylene by first cation exchanging with DHT, a low-cost, long-shelf-life, quaternary alkylammonium surfactant. The organophilic $Ti_3C_2T_z$ suspensions were stable in these solvents for at least 10 days. A solution of DHT-$Ti_3C_2T_z$ in decalin over DI water was stable for >30 days. Not only were the suspensions stable but they also appeared to be shielded from oxidation. Analysis by SEM, TEM, XRD, and ATR-FTIR reveal that the nature of $Ti_3C_2T_z$ is preserved, suggesting that this method may allow for the use of MXene in applications in which nonpolar solvents are required or preferred. As an example, this method was used to make solution-processed LLDPE nanocomposites, starting with MXene multilayers. It was found that mechanical reinforcement of the host LLDPE loaded with only 1.12 vol% DHT-functionalized $Ti_3C_2T_z$ resulted in an 11% increase in elastic moduli and a 32% increase in the maximum tensile strength. For untreated MXene composites, a 2% decrease in moduli and a

9.2% increase in maximum tensile strength were observed. In addition, the rheological properties of LLDPE were significantly modified by the presence of DHT-$Ti_3C_2T_z$ at low filler volume fraction. Filtered films made from stable suspensions of DHT-MXene in toluene showed pseudocapacitive behavior, with a maximum capacitance of 305 $F \cdot g^{-1}$ with a film thickness of >140 μm and loading of >10 $mg \cdot cm^{-2}$, indicating that this material could be commercially viable as a pseudocapacitive electrode.

EXPERIMENTAL PROCEDURES

Materials Used

To make Ti_3AlC_2, Ti, Al, and titanium carbide (TiC), powders (−325 mesh, 99.5%, Alfa Aesar) were used. DHT (80%, Alfa Chemistry) was used to treat the multilayers. DI water, ethanol, DMSO, decalin, chloroform, hexane, cyclohexane, toluene, and p-xylene (> 99% MilliporeSigma) were used as received.

Ti_3AlC_2 Synthesis

Powders of TiC, Al, and Ti in a 2:1.05:1 molar ratio were ball milled with zirconia milling balls for 24 h. This mixture was then separated from the milling balls, placed in an alumina (Al_2O_3) boat, and heated in an Al_2O_3 tube furnace at a rate of 5°C/min under continuous argon (Ar) flow to 1,350°C. After holding for 2 h at 1,350°C, the sample was allowed to cool passively. The resulting sintered, porous brick was milled and sieved with a 400 mesh sieve to obtain a particle size of <38 μm.

$Ti_3C_2T_z$ Synthesis and DHT Treatment

The $Ti_3C_2T_z$ used in this study was prepared as follows: 3 g sieved MAX powder was immersed in a 30-mL mixture of 10 wt % HF and 3.24 g LiCl for a LiCl/Ti_3AlC_2 molar ratio of 5:1. This mixture was stirred for 24 h with a polytetrafluoroethylene (PTFE)-coated magnetic stir bar at room temperature (RT) at 300 rpm. After etching, the contents were equally divided into six centrifuge tubes so that the mass of each tube was within ±0.01 g of each other. To obtain 1 g untreated MXene and 2 g DHT treated MXene, 2 of the 6 tubes were left untreated and 4 were treated with DHT.

To separate the sediment, these tubes were centrifuged at 3,500 rpm (or 2,301 RCF) for 60 s. The supernatant was discarded and replaced with DI water, for a total volume of ~40 mL in each centrifuge tube. The tubes were again centrifuged for 60 s at 3,500 rpm. After decanting the supernatant and refilling with 40 mL DI water, this procedure was repeated until a pH of 5–6, as measured by pH paper, was obtained.

After the final wash, 40 mL of a 20-mM pre-prepared solution of DHT in a 50:50 (v:v) of water and ethanol was added to the appropriate isolated sediments (made up of multilayers) and allowed to mix for 12 h at RT. After mixing, all of the powders were washed simultaneously with distilled water until no chlorine was detected by the $AgNO_3$ method.[32] The product was then vacuum filtered through a polypropylene film (Celgard LLC) and dried in vacuum at 100°C for 12 h. The resulting fine powders are hereafter referred to as DHT-MX, or simply MXene in the case of untreated powders.

Dispersion of DHT-$Ti_3C_2T_z$ in Various Solvents

Two hundred milligrams of dried DHT-MX multilayers were dispersed in 10 mL DI water, ethanol, DMSO, chloroform, decalin, hexane, cyclohexane, toluene, or p-xylene. These suspensions were briefly shaken by hand to mix them. In the case of DHT-$Ti_3C_2T_z$, dark suspensions were obtained in all of the solvents, except for water and DMSO after initial mixing by hand. Samples were then fitted with a rubber

septum and degassed for 600 s under flowing Ar before sonication in a bath sonicator for 1 h. These vials were then placed on a lab bench and left undisturbed. The stability of the various suspensions were then monitored by digital photography for 240 h (10 days). After this period, samples were transferred to 50-mL centrifuge tubes and centrifuged for 60 s at 3,500 rpm (2,301 RCF). The obtained supernatant and isolated sediments were collected, and the former were vacuum filtered for concentration analysis and subsequent characterization of the resulting films.

Synthesis of LLDPE Samples

Twenty grams of LLDPE pellets (MilliporeSigma), were added to 150 mL p-xylene in a 3-neck separable flask and degassed in a sonication bath with flowing Ar for 1 h. The reaction vessel was then heated at 125°C under reflux and mechanically stirred for 1 h before casting in Petri dishes and drying in vacuum at 100°C for 12 h. This was repeated with the addition of 1.05 g of either treated or untreated $Ti_3C_2T_z$ to obtain composite samples. After drying in vacuum, the samples were extruded at 140°C with a Filabot EX2 and the filament was collected using a Filabot Spooler. This filament was then cut by hand into pellets to be used for injection molding.

Dynamic Light Scattering (DLS)

DLS measurements were made using a NanoBrook Omni (Brookhaven Instruments) system. Colloids were placed inside a quartz cuvette, which was loaded inside the machine. Each sample was allowed to stabilize for 30 s before each measurement. Three measurements were taken for each sample, and data were then averaged before reporting.

XRD

XRD patterns were obtained with an X-ray diffractometer (Rigaku MiniFlex) with an incident Cu K_α wavelength of 1.54 Å in the range of 2°–10° 2θ or 2°–65° 2θ, with a maximum step-size of 0.02° and dwell time of 1.75 s.

XPS

Monochromatic Al-K_α X-rays with a spot size of 200 μm with a pass energy of 23.5 eV, with a step size of 0.5 eV was used to gather the high-resolution spectra.

SEM

Images and EDS maps were taken using a scanning electron microscope (Zeiss Supra 50VP) with EDS (Oxford Instruments) in secondary electron detection mode with an acceleration voltage of 20 kV and a working distance of 15.3 mm at 500× magnification.

TEM

TEM images were taken using a JEOL JEM2100 transmission electron microscope.

FTIR-ATR

Near-infrared spectra were obtained on samples with a Thermo Nicolet Nexus 870 FT-IR Spectrometer in the range of 4,000–400 cm^{-1} at RT. A background was taken and droplets of either pure solvent or DHT-MX in solvent were placed onto the ATR crystal. A total of 32 scans were taken, with a scan average of 4 for a data spacing of 0.482 cm^{-1}.

TGA

Neat and composite LLDPE pellets were tested by TGA on a TA Instruments Q50. The samples were heated at a rate of 10°C min^{-1} to 800°C under flowing Ar and

held for 0.5 h at 800°C. For the DHT-$Ti_3C_2T_z$ powder sample, the heating rate was reduced to 2°C min^{-1}.

Injection Molding and Tensile Testing of LLDPE Samples

Neat and composite ASTM D638 Type IV specimens were injection molded with a Long River desktop injection molding machine at a barrel temperature of 200°C and a mold temperature of 60°C. These samples were tested in tension at RT on an Instron 8872 Servohydraulic Testing System by following ASTM D638-14. Samples were tested at a crosshead speed of 60 mm/s for a nominal strain rate of 0.04 s^{-1}.

Rheology

Neat and composite LLDPE pellets were molded into 25-mm disks using a heated hydraulic press at 140°C. Samples were then loaded between the parallel plates of the rheometer (DHR-3, TA Instruments) and relaxed at the maximum testing temperature of 220°C. Frequency sweeps from 0.1to 100 rad/s were performed at 20°C increments down to the crystallization point. Samples remained under nitrogen for the duration of the testing. Master curves were created using time-temperature superposition.

Electrochemical Characterization

The electrochemical characterization was conducted in 3 M H_2SO_4 using a three-electrode setup (Swagelok $^1/_4$-inch T-pipe fitting) with DHT-$Ti_3C_2T_z$ film as the working electrode, overcapacitive activated carbon as the counter electrode, and Ag/AgCl in 1 M KCl solution (CHI Instruments) as the reference electrode. To prepare the working electrode, a freestanding FF of DHT-$Ti_3C_2T_z$ was punched into $^1/_8$-in diameter discs with a high mass loading of 10.12 mg/cm^2 and a thickness of 142 $\pm$ 0.7 μm. Glassy carbon (CH Instruments, model no. CHI104, 3 mm diameter) was used as the current collector. The film was soaked in the electrolyte overnight before cell assembly and testing to enable efficient electrolyte diffusion.

The electrochemical tests were performed using the potentiostat Gamry Reference 3000. CV and galvanostatic charge/discharge (GCD) tests were conducted at various scan rates (2–500 mV • s^{-1}) and current densities (0.5–10 A • g^{-1}), in a potential window from −0.7 to 0.2 V (versus Ag/AgCl).

The capacitance was calculated using the equation:

$$C = \frac{1}{2}\frac{\int I\,dV}{v \cdot m \cdot V}. \qquad \text{(Equation 4)}$$

where C, v, I, m, and V represent the capacitance (F • g^{-1}), scan rate (V • s^{-1}), current (A), mass of electrode (g), and voltage window (V), respectively. The specific capacitance was obtained from GCD curves using the expression below:

$$C = \frac{\Delta t \cdot I}{\Delta V \cdot m}. \qquad \text{(Equation 5)}$$

where I is the constant discharge current, m is the mass of the electrode, Δt is the discharge time, and ΔV is the potential window.

DATA AND CODE AVAILABILITY

All of the data are available from the corresponding author upon reasonable request.

SUPPLEMENTAL INFORMATION

Supplemental Information can be found online at https://doi.org/10.1016/j.xcrp.2020.100042.

ACKNOWLEDGMENTS

This work was funded by the Division of Materials Research of the National Science Foundation (NSF) (DMR 1740795). We would like to acknowledge and thank the members of the Drexel University College of Engineering Machine Shop, particularly Mr. Mark A. Shiber, Mr. Nick P. Catucci, and Mr. Scott Eichmann for their assistance in machining the injection molding mold.

AUTHOR CONTRIBUTIONS

M.C. and M.W.B. designed and executed the study. M.C. carried out the majority of the experiments and wrote the manuscript. Z.H. assisted in the production of nanocomposite samples, performed the rheology measurements, analyzed the data, and wrote that section of the manuscript together with his principal investigator (PI), N.J.A. V.N. performed the DLS and XPS measurements and analyzed the XPS data. R.P. performed the electrochemical measurements, analyzed the data and wrote that section of the manuscript together with his PI, V.K. M.S. collected the SEM and TEM images. All of the authors contributed to the editing of the manuscript, and M.W.B. supervised the project.

DECLARATION OF INTERESTS

The authors declare no competing interests.

Received: November 20, 2019
Revised: January 20, 2020
Accepted: February 21, 2020
Published: April 22, 2020

REFERENCES

1. Verger, L., Natu, V., Carey, M., and Barsoum, M.W. (2019). MXenes: An Introduction of Their Synthesis, Select Properties, and Applications. Trends Chem. *1*, P656–P669.
2. Natu, V., Hart, J.L., Sokol, M., Chiang, H., Taheri, M.L., and Barsoum, M.W. (2019). Edge Capping of 2D-MXene Sheets with Polyanionic Salts To Mitigate Oxidation in Aqueous Colloidal Suspensions. Angew. Chem. Int. Ed. Engl. *58*, 12655–12660.
3. Zhao, X., Vashisth, A., Prehn, E., Sun, W., Shah, S.A., Habib, T., Chen, Y., Tan, Z., Lutkenhaus, J.L., Radovic, M., and Green, M.J. (2019). Antioxidants unlock shelf-stable $Ti_3C_2T_x$ (MXene) nanosheet dispersions. Matter *1*, 513–526.
4. Konios, D., Stylianakis, M.M., Stratakis, E., and Kymakis, E. (2014). Dispersion behaviour of graphene oxide and reduced graphene oxide. J. Colloid Interface Sci. *430*, 108–112.
5. Hamilton, C.E., Lomeda, J.R., Sun, Z., Tour, J.M., and Barron, A.R. (2009). High-yield organic dispersions of unfunctionalized graphene. Nano Lett. *9*, 3460–3462.
6. Cao, Y., Feng, J., and Wu, P. (2010). Alkyl-functionalized graphene nanosheets with improved lipophilicity. Carbon N. Y. *48*, 1683–1685.
7. Tessonnier, J.-P., and Barteau, M.A. (2012). Dispersion of alkyl-chain-functionalized reduced graphene oxide sheets in nonpolar solvents. Langmuir *28*, 6691–6697.
8. Choudhary, S., Mungse, H.P., and Khatri, O.P. (2012). Dispersion of alkylated graphene in organic solvents and its potential for lubrication applications. J. Mater. Chem. *22*, 21032–21039.
9. Lim, S., Park, H., Yang, J., Kwak, C., and Lee, J. (2019). Stable colloidal dispersion of octylated Ti_3C_2-MXenes in a nonpolar solvent. Colloids Surf. A Physicochem. Eng. Asp. *579*, 123648.
10. Ghidiu, M., Lukatskaya, M.R., Zhao, M.-Q., Gogotsi, Y., and Barsoum, M.W. (2014). Conductive two-dimensional titanium carbide 'clay' with high volumetric capacitance. Nature *516*, 78–81.
11. Ghidiu, M., Kota, S., Halim, J., Sherwood, A.W., Nedfors, N., Rosen, J., Mochalin, V.N., and Barsoum, M.W. (2017). Alkylammonium cation intercalation into Ti_3C_2 (MXene): Effects on properties and ion-exchange capacity estimation. Chem. Mater. *29*, 1099–1106.
12. Ghidiu, M., Kota, S., Drozd, V., and Barsoum, M.W. (2018). Pressure-induced shear and interlayer expansion in Ti_3C_2 MXene in the presence of water. Sci. Adv. *4*, eaao6850.
13. Ghidiu, M., Halim, J., Kota, S., Bish, D., Gogotsi, Y., and Barsoum, M.W. (2016). Ion-exchange and cation solvation reactions in Ti_3C_2 MXene. Chem. Mater. *28*, 3507–3514.
14. Verger, L., Natu, V., Ghidiu, M., and Barsoum, M.W. (2019). Effect of Cationic Exchange on the Hydration and Swelling Behavior of $Ti_3C_2T_z$ MXenes. J. Phys. Chem. C *123*, 20044–20050.
15. Natu, V., Sokol, M., Verger, L., and Barsoum, M.W. (2018). Effect of Edge Charges on Stability and Aggregation of $Ti_3C_2T_z$ MXene Colloidal Suspensions. J. Phys. Chem. C *122*, 27745–27753.
16. Lukatskaya, M.R., Mashtalir, O., Ren, C.E., Dall'Agnese, Y., Rozier, P., Taberna, P.L., Naguib, M., Simon, P., Barsoum, M.W., and Gogotsi, Y. (2013). Cation intercalation and high volumetric capacitance of two-dimensional titanium carbide. Science *341*, 1502–1505.
17. Voigt, C.A., Ghidiu, M., Natu, V., and Barsoum, M.W. (2018). Anion Adsorption, $Ti_3C_2T_z$ MXene Multilayers, and Their Effect on Clay-like Swelling. J. Phys. Chem. C *122*, 23172–23179.
18. Gunstone, F.D., and Hamilton, R.J. (2001). Oleochemical Manufacture and Applications*Volume 4* (CRC Press).
19. Halim, J., Cook, K.M., Naguib, M., Eklund, P., Gogotsi, Y., Rosen, J., and Barsoum, M.W. (2016). X-ray photoelectron spectroscopy of select multi-layered transition metal carbides (MXenes). Appl. Surf. Sci. *362*, 406–417.
20. Carey, M., Hinton, Z., Sokol, M., Alvarez, N.J., and Barsoum, M.W. (2019). Nylon-6/$Ti_3C_2T_z$ MXene Nanocomposites Synthesized by in Situ Ring Opening Polymerization of ε-Caprolactam and Their Water Transport

Properties. ACS Appl. Mater. Interfaces *11*, 20425–20436.

21. Carey, M.S., Sokol, M., Palmese, G.R., and Barsoum, M.W. (2019). Water Transport and Thermomechanical Properties of $Ti_3C_2T_z$ MXene Epoxy Nanocomposites. ACS Appl. Mater. Interfaces *11*, 39143–39149.

22. Stretz, H.A., Paul, D.R., Li, R., Keskkula, H., and Cassidy, P.E. (2005). Intercalation and exfoliation relationships in melt-processed poly (styrene-co-acrylonitrile)/montmorillonite nanocomposites. Polymer (Guildf.) *46*, 2621–2637.

23. Halim, J., Moon, E.J., Eklund, P., Rosen, J., Barsoum, M.W., and Ouisse, T. (2018). Variable range hopping and thermally activated transport in molybdenum-based MXenes. Phys. Rev. B *98*, 104202.

24. Maleski, K., Mochalin, V.N., and Gogotsi, Y. (2017). Dispersions of Two-Dimensional Titanium Carbide MXene in Organic Solvents. Chem. Mater. *29*, 1632–1640.

25. Coleman, J.N. (2009). Liquid-phase exfoliation of nanotubes and graphene. Adv. Funct. Mater. *19*, 3680–3695.

26. Haynes, and William, M. (2014). CRC Handbook of Chemistry and Physics (CRC Press).

27. Chevigny, C., Dalmas, F., Di Cola, E., Gigmes, D., Bertin, D., Boué, F., and Jestin, J. (2010). Polymer-grafted-nanoparticles nanocomposites: dispersion, grafted chain conformation, and rheological behavior. Macromolecules *44*, 122–133.

28. Akuzum, B., Maleski, K., Anasori, B., Lelyukh, P., Alvarez, N.J., Kumbur, E.C., and Gogotsi, Y. (2018). Rheological characteristics of 2D titanium carbide (MXene) dispersions: a guide for processing MXenes. ACS Nano *12*, 2685–2694.

29. Lukatskaya, M.R., Kota, S., Lin, Z., Zhao, M.-Q., Shpigel, N., Levi, M.D., Halim, J., Taberna, P.-L., Barsoum, M.W., Simon, P., and Gogotsi, Y. (2017). Ultra-high-rate pseudocapacitive energy storage in two-dimensional transition metal carbides. Nat. Energy *2*, 17105.

30. Mashtalir, O., Naguib, M., Mochalin, V.N., Dall'Agnese, Y., Heon, M., Barsoum, M.W., and Gogotsi, Y. (2013). Intercalation and delamination of layered carbides and carbonitrides. Nat. Commun. *4*, 1716.

31. Naguib, M., Unocic, R.R., Armstrong, B.L., and Nanda, J. (2015). Large-scale delamination of multi-layers transition metal carbides and carbonitrides "MXenes". Dalton Trans. *44*, 9353–9358.

32. Yoder, L. (1919). Adaptation of the Mohr Volumetric Method to General Determinations of Chlorine. Ind. Eng. Chem. *11*, 755.

33. Hu, M., Li, Z., Zhang, H., Hu, T., Zhang, C., Wu, Z., and Wang, X. (2015). Self-assembled $Ti_3C_2T_x$ MXene film with high gravimetric capacitance. Chem. Commun. (Camb.) *51*, 13531–13533.

34. Dall'Agnese, Y., Lukatskaya, M.R., Cook, K.M., Taberna, P.L., Gogotsi, Y., and Simon, P. (2014). High capacitance of surface-modified 2D titanium carbide in acidic electrolyte. Electrochem. Commun. *48*, 118–122.

35. Ling, Z., Ren, C.E., Zhao, M.Q., Yang, J., Giammarco, J.M., Qiu, J., Barsoum, M.W., and Gogotsi, Y. (2014). Flexible and conductive MXene films and nanocomposites with high capacitance. Proc. Natl. Acad. Sci. USA *111*, 16676–16681.